Extending the fundamental imaging-depth limit of multi-photon microscopy by imaging with photo-activatable fluorophores

Zhixing Chen, Lu Wei, Xinxin Zhu, and Wei Min*

Department of Chemistry, Columbia University, New York, New York 10027, USA
*wm2256@columbia.edu

Abstract: It is highly desirable to be able to optically probe biological activities deep inside live organisms. By employing a spatially confined excitation via a nonlinear transition, multiphoton fluorescence microscopy has become indispensable for imaging scattering samples. However, as the incident laser power drops exponentially with imaging depth due to scattering loss, the out-of-focus fluorescence eventually overwhelms the in-focal signal. The resulting loss of imaging contrast defines a fundamental imaging-depth limit, which cannot be overcome by increasing excitation intensity. Herein we propose to significantly extend this depth limit by multiphoton activation and imaging (MPAI) of photo-activatable fluorophores. The imaging contrast is drastically improved due to the created disparity of bright-dark quantum states in space. We demonstrate this new principle by both analytical theory and experiments on tissue phantoms labeled with synthetic caged fluorescein dye or genetically encodable photoactivatable GFP.

©2012 Optical Society of America

OCIS codes: (180.4315) Nonlinear microscopy; (180.2520) Fluorescence microscopy; (190.4180) Multiphoton processes; (160.4330) Nonlinear optical materials; (170.6280) Spectroscopy, fluorescence and luminescence; (170.5810) Scanning microscopy.

References and links

1. S. W. Hell and J. Wichmann, "Breaking the diffraction resolution limit by stimulated emission: stimulated-emission-depletion fluorescence microscopy," Opt. Lett. **19**(11), 780–782 (1994).
2. E. Betzig, G. H. Patterson, R. Sougrat, O. W. Lindwasser, S. Olenych, J. S. Bonifacino, M. W. Davidson, J. Lippincott-Schwartz, and H. F. Hess, "Imaging intracellular fluorescent proteins at nanometer resolution," Science **313**(5793), 1642–1645 (2006).
3. S. T. Hess, T. P. Girirajan, and M. D. Mason, "Ultra-high resolution imaging by fluorescence photoactivation localization microscopy," Biophys. J. **91**(11), 4258–4272 (2006).
4. M. J. Rust, M. Bates, and X. Zhuang, "Sub-diffraction-limit imaging by stochastic optical reconstruction microscopy (STORM)," Nat. Methods **3**(10), 793–796 (2006).
5. W. Denk, J. H. Strickler, and W. W. Webb, "Two-photon laser scanning fluorescence microscopy," Science **248**(4951), 73–76 (1990).
6. W. R. Zipfel, R. M. Williams, and W. W. Webb, "Nonlinear magic: multiphoton microscopy in the biosciences," Nat. Biotechnol. **21**(11), 1369–1377 (2003).
7. F. Helmchen and W. Denk, "Deep tissue two-photon microscopy," Nat. Methods **2**(12), 932–940 (2005).
8. R. Yuste, ed., *Imaging: A Laboratory Manual* (Cold Spring Harbor Laboratory Press, 2010)
9. P. Theer, M. T. Hasan, and W. Denk, "Two-photon imaging to a depth of 1000 microm in living brains by use of a Ti:Al2O3 regenerative amplifier," Opt. Lett. **28**(12), 1022–1024 (2003).
10. P. Theer and W. Denk, "On the fundamental imaging-depth limit in two-photon microscopy," J. Opt. Soc. Am. A **23**(12), 3139–3149 (2006).
11. D. Kobat, N. G. Horton, and C. Xu, "In vivo two-photon microscopy to 1.6-mm depth in mouse cortex," J. Biomed. Opt. **16**(10), 106014 (2011).
12. N. J. Durr, C. T. Weisspfennig, B. A. Holfeld, and A. Ben-Yakar, "Maximum imaging depth of two-photon autofluorescence microscopy in epithelial tissues," J. Biomed. Opt. **16**(2), 026008 (2011).
13. J. Ying, F. Liu, and R. R. Alfano, "Spatial distribution of two-photon-excited fluorescence in scattering media," Appl. Opt. **38**(1), 224–229 (1999).

#166548 - $15.00 USD Received 12 Apr 2012; revised 18 Jun 2012; accepted 19 Jun 2012; published 30 Jul 2012
(C) 2012 OSA

14. N. Ji, D. E. Milkie, and E. Betzig, "Adaptive optics via pupil segmentation for high-resolution imaging in biological tissues," Nat. Methods **7**(2), 141–147 (2010).
15. M. Rueckel, J. A. Mack-Bucher, and W. Denk, "Adaptive wavefront correction in two-photon microscopy using coherence-gated wavefront sensing," Proc. Natl. Acad. Sci. U.S.A. **103**(46), 17137–17142 (2006).
16. D. Kobat, M. E. Durst, N. Nishimura, A. W. Wong, C. B. Schaffer, and C. Xu, "Deep tissue multiphoton microscopy using longer wavelength excitation," Opt. Express **17**(16), 13354–13364 (2009).
17. H. Hama, H. Kurokawa, H. Kawano, R. Ando, T. Shimogori, H. Noda, K. Fukami, A. Sakaue-Sawano, and A. Miyawaki, "Scale: a chemical approach for fluorescence imaging and reconstruction of transparent mouse brain," Nat. Neurosci. **14**(11), 1481–1488 (2011).
18. A. Leray, K. Lillis, and J. Mertz, "Enhanced background rejection in thick tissue with differential-aberration two-photon microscopy," Biophys. J. **94**(4), 1449–1458 (2008).
19. M. Fernández-Suárez and A. Y. Ting, "Fluorescent probes for super-resolution imaging in living cells," Nat. Rev. Mol. Cell Biol. **9**(12), 929–943 (2008).
20. J. Lippincott-Schwartz and G. H. Patterson, "Photoactivatable fluorescent proteins for diffraction-limited and super-resolution imaging," Trends Cell Biol. **19**(11), 555–565 (2009).
21. M. Heilemann, P. Dedecker, J. Hofkens, and M. Sauer, "Photoswitches: key molecules for subdiffraction-resolution fluorescence imaging and molecular quantification," Laser Photon. Rev. **3**(1-2), 180–202 (2009).
22. H. L. Lee, S. J. Lord, S. Iwanaga, K. Zhan, H. Xie, J. C. Williams, H. Wang, G. R. Bowman, E. D. Goley, L. Shapiro, R. J. Twieg, J. Rao, and W. E. Moerner, "Superresolution imaging of targeted proteins in fixed and living cells using photoactivatable organic fluorophores," J. Am. Chem. Soc. **132**(43), 15099–15101 (2010).
23. J. Fölling, V. Belov, R. Kunetsky, R. Medda, A. Schönle, A. Egner, C. Eggeling, M. Bossi, and S. W. Hell, "Photochromic rhodamines provide nanoscopy with optical sectioning," Angew. Chem. Int. Ed. Engl. **46**(33), 6266–6270 (2007).
24. D. Kleinfeld, P. P. Mitra, F. Helmchen, and W. Denk, "Fluctuations and stimulus-induced changes in blood flow observed in individual capillaries in layers 2 through 4 of rat neocortex," Proc. Natl. Acad. Sci. U.S.A. **95**(26), 15741–15746 (1998).
25. T. J. Mitchison, K. E. Sawin, J. A. Theriot, K. Gee, and A. Mallavarapu, "Caged fluorescent probes," Methods Enzymol. **291**, 63–78 (1998).
26. G. H. Patterson and J. Lippincott-Schwartz, "A photoactivatable GFP for selective photolabeling of proteins and cells," Science **297**(5588), 1873–1877 (2002).
27. M. Schneider, S. Barozzi, I. Testa, M. Faretta, and A. Diaspro, "Two-photon activation and excitation properties of PA-GFP in the 720-920-nm region," Biophys. J. **89**(2), 1346–1352 (2005).
28. Y. Zhao, Q. Zheng, K. Dakin, K. Xu, M. L. Martinez, and W.-H. Li, "New caged coumarin fluorophores with extraordinary uncaging cross sections suitable for biological imaging applications," J. Am. Chem. Soc. **126**(14), 4653–4663 (2004).
29. R. Ando, H. Mizuno, and A. Miyawaki, "Regulated fast nucleocytoplasmic shuttling observed by reversible protein highlighting," Science **306**(5700), 1370–1373 (2004).
30. M.-Q. Zhu, G.-F. Zhang, C. Li, M. P. Aldred, E. Chang, R. A. Drezek, and A. D. Q. Li, "Reversible two-photon photoswitching and two-photon imaging of immunofunctionalized nanoparticles Targeted to Cancer Cells," J. Am. Chem. Soc. **133**(2), 365–372 (2011).
31. L. Wei, Z. Chen, and W. Min, "Stimulated emission reduced fluorescence microscopy: a concept for extending the fundamental depth limit of two-photon fluorescence imaging," Biomed. Opt. Express **3**(6), 1465–1475 (2012).

1. Introduction

Our ability to study the microscopic world has been revolutionized by advances in optical imaging technology. However, compared to electron microscopy and magnetic resonance imaging, optical microscopy suffers intrinsically from relatively coarse spatial resolution and superficial penetration depth. As one can imagine, resolution and penetration are two fundamentally coupled physical properties. While the diffraction-limited resolution barrier has been broken by a number of super-resolution fluorescence techniques such as STED, (F)PALM and STORM [1–4], the deepest penetration into scattering samples with sub-cellular resolution is achieved currently by multi-photon microscopy. By employing a nonlinear intensity-dependent optical excitation, multi-photon fluorescence is generated primarily at the focal volume where the probability of absorbing two (or more) photons by the same molecule at the same time is the highest, enabling an intrinsic 3D optical sectioning capability [5, 6]. Such a spatially confined excitation scheme thus permits the capture of fluorescence photons emitted and then scattered from the focus by a wide-field non-descanned detector, thereby dramatically increasing the detection sensitivity of scattered

#166548 - $15.00 USD Received 12 Apr 2012; revised 18 Jun 2012; accepted 19 Jun 2012; published 30 Jul 2012
(C) 2012 OSA

signals. This profound feature ultimately leads to a significant imaging depth into scattering samples (more than three times deeper than that of one-photon confocal microscopy) [7, 8].

As many other optical imaging modalities, a fundamental imaging-depth limit still exists for multiphoton fluorescence microscopy when imaging scattering samples labeled with fluorophores in 3D volume [9–13]. Here we take Fig. 1 as an example: the two-photon fluorescence images of fluorescent beads embedded in a turbid 3D sample quickly vanish with the depth when using constant laser power (Fig. 1a). This seemingly shallow cut-off depth is not the ultimate maximum, as imaging can actually be performed much deeper provided that the incident laser power can be elevated accordingly to compensate for the scattering loss (Fig. 1b). However, such a signal-promoting procedure comes at the cost of deteriorating imaging contrast: at a certain depth, the target beads can no longer be identified from the overwhelming background. Formally, the depth where the in-focus signal and the out-of-focus background are equal to each other is defined as the fundamental imaging-depth limit [10]. Note that the conventional optical sectioning picture that multiphoton fluorescence is generated only within the focal volume breaks down here, because the exponential increase of the incident laser power eventually outstrips the power-law fall-off of the excitation efficiency out-of-focus. Obviously, further increasing incident laser power cannot overcome this contrast-rendered imaging-depth limit.

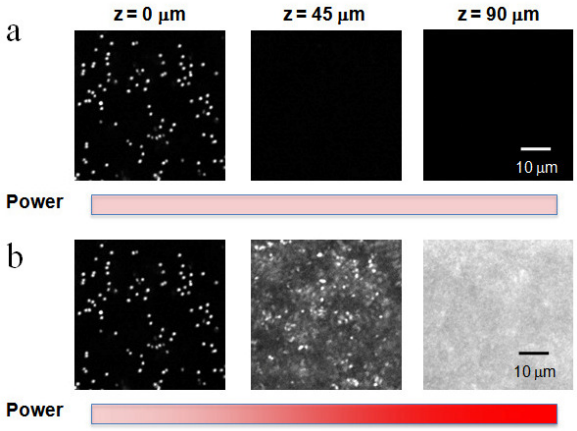

Fig. 1. Fundamental imaging-depth limit of multi-photon fluorescence microscopy. (a) Images of a tissue phantom consisting of 5% intralipid, 1 μm fluorescent beads (Invitrogen F8765) and 1% agarose gel under a constant excitation laser power. Two-photon fluorescence signal quickly attenuates with the imaging depth. (b) Images of the same sample using a compensative higher laser power to maintain the signal strength at different depths. The resulting images, although showing signals deeper into the sample, suffer from a loss of contrast as the out-of-focus background grows. The fundamental imaging-depth limit is defined when the in-focus signal and the out-of-focus background are equal to each other.

Largely driven by the desire to perform *in vivo* deep tissue imaging, there have been tremendous efforts in improving the imaging depth of multiphoton microscopy. Several strategies have been explored, such as adaptive optics designed to pre-compensate for the scattering loss [14,15], imaging with longer excitation wavelength [16], chemical cleaning reagent [17], and differential aberration imaging [18]. However, relatively little work has been published on exploring novel imaging probes as a way of improving the image contrast or extending the imaging-depth limit.

Herein we present the application of photo-activatable fluorophores (PAFs) to extend the fundamental imaging-depth limit. PAFs are powerful imaging probes for tracking molecular and cellular dynamics with high temporal resolution, and have recently emerged as the key players in super-resolution fluorescence microscopy [2–4,19–22] including nanoscopy with

#166548 - $15.00 USD Received 12 Apr 2012; revised 18 Jun 2012; accepted 19 Jun 2012; published 30 Jul 2012
(C) 2012 OSA

optical sectioning capability [23]. Unlike traditional fluorophores which always remain in their bright states, PAFs permit photo-induced transitions from dark states to bright states. By preferentially inducing the bright states into the focus and dark states into the out-of-focus background, multiphoton activation and imaging (MPAI) of PAFs can significantly enhance the imaging contrast and extend the depth limit of multiphoton microscopy. We demonstrate our proposal by both analytical theory and imaging experiments on tissue phantoms labeled with synthetic caged fluorescein dye or photoactivatable green fluorescent protein. Therefore, by offering the additional on-off molecular quantum states, PAFs seem to be capable of both breaking the diffraction-limited spatial resolution and extending the imaging-depth limit.

2. Results and discussions

2.1 The fundamental imaging-depth limit of two-photon microscopy

Let us first frame the problem of deep two-photon imaging with regular fluorophores. The fundamental imaging-depth limit can be defined as the point where the in-focus signal and the out-of-focus background are equal [9–13]:

$$\left(\frac{S}{B}\right)_{regular} = \frac{\int_{V_{in}}\int_0^{\tau} C_S(r,z) I_i^2(r,z,t)\mathrm{d}t\mathrm{d}V}{\int_{V_{out}}\int_0^{\tau} C_B(r,z) I_i^2(r,z,t)\mathrm{d}t\mathrm{d}V} = 1, \qquad (1)$$

where V_{in}, is the focal volume at the focal plane, V_{out}, is the total sample volume along the light path but excluding the volume at the focal plane, r, is the distance from the optical axis, z, is the axial distance from the tissue surface, C, is the local fluorophore concentration, I_i is the local imaging laser intensity, and τ, is the pixel dwell time during imaging. We assume that there is no fluorophore saturation or photobleaching and that the fluorescence collection efficiencies at the wide-field detector are identical for the signal and the background.

We can now analyze the laser intensity distribution within a scattering sample. In a typical scenario where the fluorophores are distributed throughout the sample volume, the number of out-of-focus fluorophores is almost always much larger than that of the in-focus ones $\int_{V_{out}} C_B(r,z)\mathrm{d}V >> \int_{V_{in}} C_S(r,z)\mathrm{d}V$. Therefore, at the fundamental imaging-depth limit as defined in Eq. (1), $I_i^2(r,z)|_{V_{in}}$ at the focus should be much larger than the out-of-focus counterpart $I_i^2(r,z)|_{V_{out}}$, despite of the scattering loss. Indeed, in the simple condition of homogeneous fluorophore distribution, i.e., $C_B(r,z) = C_B(r,z)$, $\int_V\int_0^{\tau} I_i^2(r,z,t)\mathrm{d}t\mathrm{d}V$ will be identical between the background and the signal, and consequently, the integral of $I_i^2(r,z)$ over a subset layers of the out-of-focus volume (e.g., $\int_{out} I_i^2(r,z,)\mathrm{d}r$ for any z) will be smaller than that over the focus.

2.2 Reducing the background fluorophore concentration alone can improve the depth limit

Although the sample scattering is seemingly the origin of the limited light penetration, the above theoretical framework suggests that the concentration of background fluorophores should play an important role in determining the depth limit. To separate these two effects, we constructed and imaged a set of "two-layer" samples (Fig. 2). 0-5% intralipid emulsions were used as they closely mimic the response of biological tissues to near infrared light. In the absence of scattering intralipid, increasing fluorescein concentration in the background does not affect the two-photon imaging quality of the target fluorescent beads. In contrast, when the scattering effects are strong enough (e.g., 2% and 5% intralipid), the two-photon imaging contrast becomes anti-correlated with the background fluorescein concentration.

#166548 - $15.00 USD Received 12 Apr 2012; revised 18 Jun 2012; accepted 19 Jun 2012; published 30 Jul 2012
(C) 2012 OSA

Thus, both strong sample scattering and abundant background fluorophores are necessary conditions for the limited imaging-depth. Sample scattering alone does not create poor imaging contrast. As an important insight, images presented in Fig. 2 suggest that, simply reducing the background dye concentration while maintaining the high intralipid content still allows imaging the target beads with increased contrast.

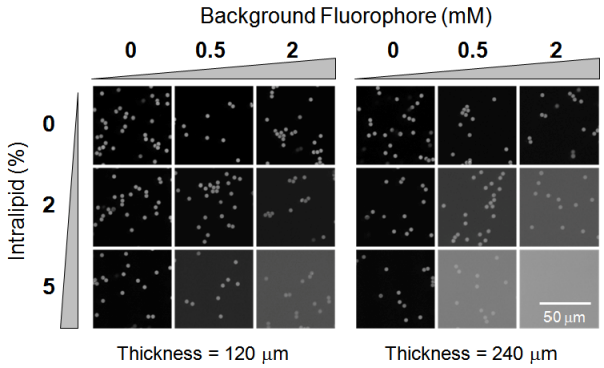

Fig. 2. Imaging contrast of multi-photon microscopy depends on both sample scattering and background fluorophore concentration. A set of "two-layer" samples (fluorescent beads were placed on a glass coverslip as the target, while a thick layer of mixed fluorescein dye solution and scattering intralipids was inserted as the background between the target and the objective.) with varying intralipid contents and background dye concentrations were imaged using a two-photon microscope. The laser power was set higher accordingly when a more scattering sample was imaged. At a given background layer thickness, image contrast deteriorates only when both a significant background turbidity and a dense background fluorophore staining are present. Imaging contrast further deteriorates when thicker background layers were applied.

2.3 Theoretical framework of MPAI using dynamic PAFs

Inspired by the above insight, we envision a way to preferentially keep the background fluorophores in the dark states by using PAFs which have to be activated first by multiphoton process before excited by another multiphoton process. Two different modes of experiments are possible: simultaneous or sequential activation and imaging. When PAFs are being activated and imaged by I_a and I_i (one same activation-imaging laser or two combined lasers, where I_a is the local intensity of the activation laser) simultaneously, $C(r,z)$ in Eq. (1) should be replaced by $A(r,z,t)$, the time-dependent concentration of the PAFs in the bright state. Quantitatively, $A(r,z,t)$ will be the product of $C(r,z)$ and the time-dependent multiphoton activation yield, $\eta(t)$:

$$A(r,z,t) = C(r,z)\eta(r,z,t). \tag{2}$$

In the simplest condition, $\eta(t)$ follows a first-order chemical kinetics:

$$\eta(t) = 1 - \exp\left[-\sigma I_a^2(r,z,t)t\right] \quad 0 \le t \le \tau, \tag{3}$$

with a rate constant being proportional to $I_a^2(r,z)$ of the activation laser and the two-photon activation cross section, σ. Alternatively, we describe the sequential mode in which activation by I_a and imaging by I_i are performed at two laser wavelengths in sequential raster scans: $A(r,z) = C(r,z)\eta(r,z,\psi)$, where ψ is the pixel dwell time of the multiphoton activation scanning process, and the resulting $A(r,z)$ becomes time independent to the subsequent imaging process.

#166548 - $15.00 USD Received 12 Apr 2012; revised 18 Jun 2012; accepted 19 Jun 2012; published 30 Jul 2012
(C) 2012 OSA

When the timescale for PAFs to diffuse or transport out of the laser focal volume is shorter than the frame acquisition time, the accumulation of the activated fluorophores in the background during the scanning process could be neglected. This dynamic condition is rather common, as exemplified by *in vivo* blood vessel imaging in which fluorophores are injected into the circulatory systems of small animals [24]. Hence, the signal-to-background ratio for dynamic PAFs can be expressed as

$$\left(\frac{S}{B}\right)_{PAFs} = \frac{\int_{V_{in}}\int_0^{\tau} C_S(r,z) I_i^2 \left[1-e^{\sigma I_a^2(r,z,t)t}\right] I_i^2(r,z,t)\mathrm{d}t\mathrm{d}V}{\int_{V_{out}}\int_0^{\tau} C_B(r,z)\left[1-e^{\sigma I_a^2(r,z,t)t}\right] I_i^2(r,z,t)\mathrm{d}t\mathrm{d}V}. \quad (4)$$

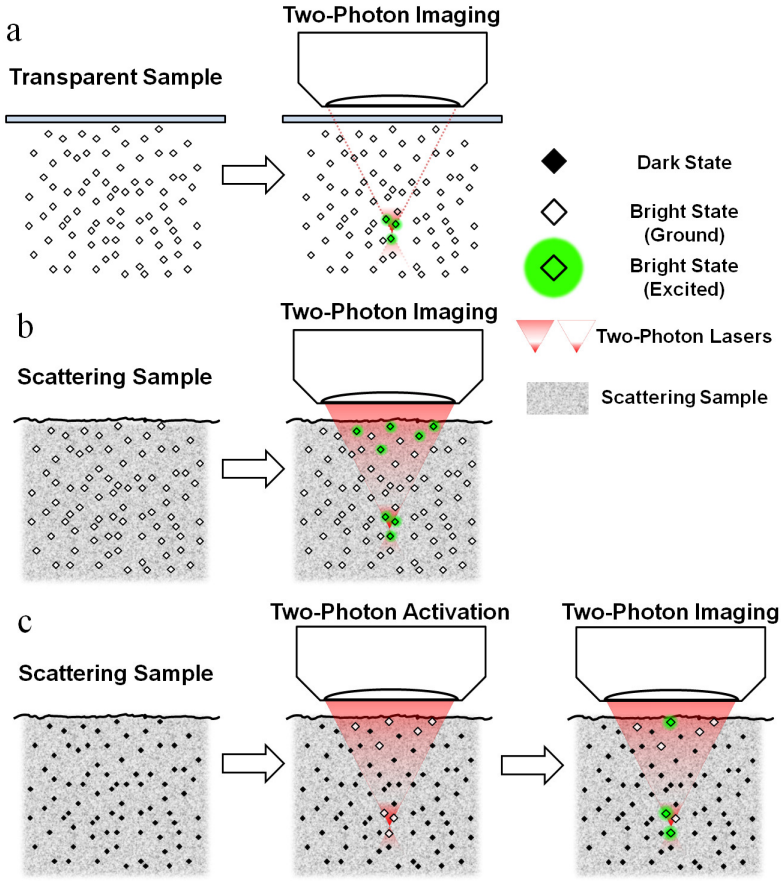

Fig. 3. Principle of multiphoton activation and imaging (MPAI). (a) When imaging transparent samples, fluorescence is only generated at the laser focus where the intensity is the highest. (b) When imaging deep into scattering samples, substantial laser intensities are distributed out of focus, generating background fluorescence that is comparable to or even stronger than the in-focus signal. (c) When imaging with PAFs which are originally in the dark state, the multiphoton activation will switch on a higher percentage of PAFs at focus than those out-of-focus. Such a spatial disparity of dark-bright transitions would lead to a significantly decreased background fluorescence in the subsequent imaging.

As was analyzed earlier, the laser intensity at the focus is much higher than its out-of-focus counterparts at the imaging-depth limit defined by Eq. (1). This would lead to a much higher dark-to-bright conversion yield at the focus: $\eta_S(r,z,t) > \eta_B(r,z,t),$, under a proper

#166548 - $15.00 USD Received 12 Apr 2012; revised 18 Jun 2012; accepted 19 Jun 2012; published 30 Jul 2012
(C) 2012 OSA

pixel dwell time with a non-saturating activation yield. Consequently, we expect a much improved signal-to-background ratio for PAFs than for regular fluorophores:

$$(S/B)_{PAFs} > (S/B)_{regular}. \tag{5}$$

It is constructive to note that, after the photoactivation (with a non-saturating activation yield), the number of in-focus activated PAFs become comparable to the total number of the activated ones out-of-focus:

$$\left(\frac{N_S}{N_B}\right)_{activated} = \frac{\int_{V_{in}}\int_0^\tau C_S(r,z)\left[1-e^{\sigma I_a^2(r,z,t)\tau}\right]\mathrm{d}t\mathrm{d}V}{\int_{V_{out}}\int_0^\tau C_B(r,z)\left[1-e^{\sigma I_a^2(r,z,t)\tau}\right]\mathrm{d}t\mathrm{d}V} \approx \cdot \frac{\int_{V_{in}}\int_0^\tau C_S(r,z)I_a^2(r,z,t)\mathrm{d}t\mathrm{d}V}{\int_{V_{out}}\int_0^\tau C_B(r,z)I_a^2(r,z,t)\mathrm{d}t\mathrm{d}V} = 1. \tag{6}$$

Compared to the regular dye case in which:

$$\left(\frac{N_S}{N_B}\right)_{regular} = \frac{\int_{V_{in}} C_S(r,z)\mathrm{d}V}{\int_{V_{out}} C_B(r,z)\mathrm{d}V} \approx \frac{V_{in}}{V_{out}} \ll 1. \tag{7}$$

Equation (6) clearly indicates that the bright states are preferentially induced at the focus whereas the out-of-focus PAFs mostly remain in dark states. As shown in Fig. 3, such a remarkable disparity of bright-dark states in space would significantly reduce the background contribution from out-of-focus fluorophores.

2.4 Experimental demonstration of MPAI using a caged organic dye

Caged fluorescein, resorufin and rhodamine are the first developed small organic PAFs. They have been applied to study the assembly of tubulin, hydrodynamic flows and cell lineage during embryo development [25]. Here we use the caged fluorescein, which is commercially available, as a proof-of-principle. Figure 4(a) shows the photo-uncaging reaction of caged fluorescein. The dark state can be activated to the bright state by illuminating with UV light as shown by the absorption and fluorescence spectra and uncaging kinetics in Fig. 4(b). For our two-photon application, laser pulses at 750 nm can uncage the protective groups and subsequently excite the bright state. Therefore only one laser is needed in this simultaneous mode, i.e., $I_a = I_i$. We again constructed "two-layer" samples. The target object, a droplet of caged fluorescein solution, was placed on a glass coverslip, and a thick layer made of mixed scattering beads and caged fluorescein was inserted between the target and the objective. Control two-layer samples exhibit same physical parameters except for the use of regular fluorescein in both the target droplets and the out-of-focus background layers.

Figure 4(c)-(f) show the comparison between $(S/B)_{regular}$ and $(S/B)_{PAFs}$ in our tissue phantoms labeled with dynamic fluorophores. Using control samples, we first determined the proper concentrations of scattering and dye species in the background layer so that imaging with regular fluorescein is approaching the fundamental imaging-depth limit with $(S/B)_{regular} \approx 1.2$ (Fig. 4c). We then switched to the corresponding PAFs sample. To accommodate the relatively slow photo-activation of caged fluorescein, a long pixel dwell time of ~1.0 ms was used to obtain enough fluorescence signals. The resulting $(S/B)_{PAFs}$ is found to be about 20 in Fig. 4(d), exhibiting a significant improvement of imaging contrast. Encouraged by this, we further elevated the background dye concentration by a factor of 3 for both control and PAFs samples in Fig. 4(e) and 4(f). As expected, $(S/B)_{regular} \approx 1.3$ is now beyond what the depth limit permits. In contrast, the corresponding PAFs sample exhibits a remarkable $(S/B)_{PAFs} \approx 8$.

#166548 - $15.00 USD Received 12 Apr 2012; revised 18 Jun 2012; accepted 19 Jun 2012; published 30 Jul 2012
(C) 2012 OSA

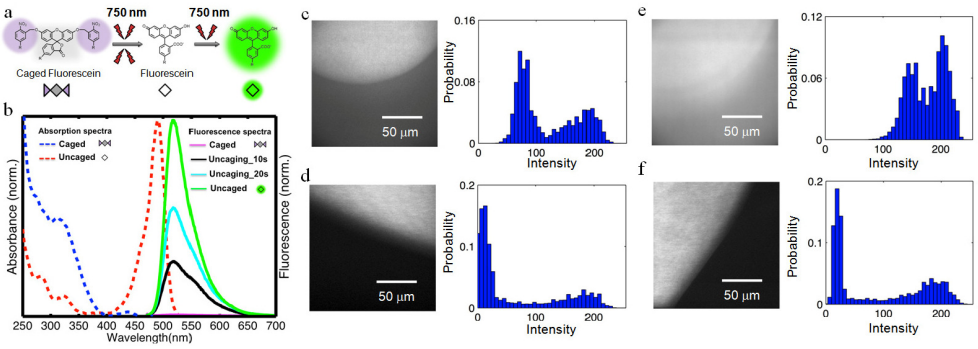

Fig. 4. Experimental demonstration of MPAI with caged fluorescein. (a) CMNB (5-carboxymethoxy-2-nitrobenzyl) caging groups of CMNB-caged fluorescein could be cleaved by a 750 nm pulsed laser, leading to the formation of fluorescein in the bright state, which could be excited by the same laser to emit fluorescence. (b) Absorption and fluorescence spectra of caged fluorescein and uncaged fluorescein, with the activation kinetics under UV illumination. A ~100-fold fluorescence enhancement was observed after a complete activation. (c-f) Imaging "two-layer" samples (Fig. 7.) where the targets are 2 μL droplets of 1 mM dye solution and the background layers (120 μm thick) consist of scattering polystyrene beads (0.9 μm) and dye solution (1 mM for (c) and (d), 3 mM for (e) and (f)). Boundaries of liquid droplets cross the field of view so that the darker parts correspond to the background while the brighter parts represent the sum of the signal and the background. When the imaging depth-limit is reached for regular fluorescein in (c) with a S/B of about 1.2, a 20-times improvement is achieved for caged fluorescein in (d). With a three folds more dyes in the background layer of (e) and (f), imaging contrast becomes extremely poor for regular fluorescein, while the caged fluorescein still offers a S/B of about 8.

2.5 Theoretical framework of MPAI using static PAFs

If PAFs are rather static during the entire frame acquisition, we then need to consider the spatio-temporal accumulation of the activated fluorophore in out-of-focus background during the raster scanning. In this scenario, while η_S of the signal remains the same as in Eqs. (2)-(4), the effective activation time for η_B will be longer than the pixel dwell time, τ, by a factor of, $f(z)$, which scales with the z-dependent laser beam area. The result of static PAFs hence becomes:

$$\left(\frac{S}{B}\right)_{PAFs} = \frac{\int_{V_{in}}\int_0^{\tau} C_S(r,z)\eta_S(r,z,t)I_i^2(r,z,t)\mathrm{d}t\mathrm{d}V}{\int_{V_{out}}\int_0^{\tau} C_B(r,z)\eta_B(r,z,f(z)\cdot\tau)I_i^2(r,z,t)\mathrm{d}t\mathrm{d}V}. \tag{8}$$

Thus, due to the accumulation of the activated fluorophores during laser scanning, the out-of-focus background will be higher here compared to that from dynamic PAFs described in Eq. (4). In the condition of low photo-activation yield, we have the following approximation

$$\frac{\eta_S(r,z,\tau)}{\eta_B(r,z,f(z)\cdot\tau)} \approx \frac{I_a^2(r,z)|_{V_{in}}}{f(z)\cdot I_a^2(r,z)|_{V_{out}}} \approx \frac{\int_{in} I_i^2(r,z)\mathrm{d}r}{\int_{out} I_a^2(r,z)\mathrm{d}r} > 1. \tag{9}$$

From the earlier analysis of laser intensity distribution at the depth limit defined in Eq. (1), we have inferred that $\int_{in} I^2(r,z,)\mathrm{d}r > \int_{out} I^2(r,z)\mathrm{d}r$ for all z layers. Consequently, the final activation yield will be higher at the focus than in the background. Therefore, the signal-to-background ratio using static PAFs is still higher in Eq. (8) than that with regular fluorophores in Eq. (1).

#166548 - $15.00 USD Received 12 Apr 2012; revised 18 Jun 2012; accepted 19 Jun 2012; published 30 Jul 2012
(C) 2012 OSA

2.6 Experimental demonstration of MPAI using a photo-activatable fluorescent protein

PAFs also include several fluorescent proteins that can be genetically encoded and fused to other proteins of interest for *in vivo* imaging of cells and animals. Photoactivatable green fluorescent protein (pa-GFP) is the first member of this family of optical highlighters [26]. As shown in Fig. 5(a), pa-GFP can be turned on from its initial dark state by two-photon activation in the 750~850 nm range, and the resulting bright state can be readily imaged in the 900~950 nm range [27].

We prepared tissue phantoms by embedding the *E. coli* cells expressing fluorescent protein into 3D agarose gel. The resulting sample is highly scattering due to the densely packed *E. coli* cells. The PAFs in this sample are considered static, as the cells are stationary within the agarose gel. As demonstrated in Fig. 5(b) and 5(c), while the out-of-focus background is overwhelming for cells expressing regular GFP at a depth of 100 μm, MPAI of cells expressing pa-GFP at the same depth offers a satisfactory image contrast. Thus, we have experimentally demonstrated the ability of MAPI in extending the fundamental imaging-depth limit of two-photon fluorescence microscopy.

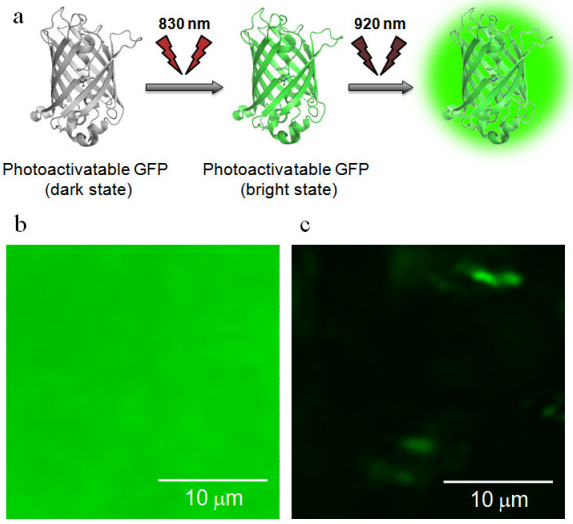

Fig. 5. Experimental demonstration of MPAI with pa-GFP. (a) pa-GFP could be activated by a pulsed laser at 830 nm to its bright state, which could be further excited by a 920 nm pulsed laser to emit fluorescence. (b, c) Deep imaging comparison of 3D turbid samples made of *E. coli* cells expressing free regular GFP (b) or pa-GFP (c) embedded in 2% agarose gel with the same cell densities. While out-of-focus background is overwhelming when imaging *E. coli* expressing regular GFP at a 100 μm depth inside the gel, MPAI with pa-GFP at the same depth offers a satisfactory image contrast.

3. Methods and materials

3.1 Sample preparation

Fluorescent beads were purchased from Invitrogen (F8765: green/yellow 1.0 μm beads; F8859: green/yellow 4.0 μm beads). Fluorescein (Sigma 46960) and CMNB-Caged Carboxyfluorescein (Invitrogen C-20050) were prepared into 10 mM stock solution in DMSO before diluting to final concentrations. Intralipid (Sigma I141) or non-fluorescent polystyrene beads (Sigma CLB9) were used as the scattering species. “Two-layer” samples in Figs. 2 and 4 were prepared as shown in Figs. 6 and 7: An imaging spacer with a 120 μm thickness (Sigma S7935) was pasted onto a piece of micro coverglass (VWR 48393-220). Inside the spacer, 5 μL of material serving as the scattering background was added. For the activation-

#166548 - $15.00 USD Received 12 Apr 2012; revised 18 Jun 2012; accepted 19 Jun 2012; published 30 Jul 2012
(C) 2012 OSA

imaging experiments of fluorescein and caged fluorescein (Fig. 4c-f), suspension of non-fluorescent 0.9 μm polystyrene beads (Sigma CLB9) was sonicated and diluted (1:5) into 50% glycerol solution with fluorescein or caged fluorescein at a concentration of 1 mM or 3 mM to serve as the scattering background. The background material was then sealed inside the spacer by another piece of micro coverglass on top, giving a sandwich-like background sample. Imaging targets (fluorescent beads or dye droplets) were placed on top of the glass sandwich before imaging. Glycerol solutions were used to minimize evaporation of solvent during the imaging process. In bacteria imaging experiments, BL21 *E. coli* strains expressing pa-GFP (Addgene plasmid 11911) and Dronpa-3 (a regular GFP version for control imaging, MBL International Corporation) were harvested by centrifugation, resuspended and embedded inside an imaging spacer using 2% agarose gel. *E. coli* densities of different samples were calibrated based on OD600 measurement to achieve the consistent scattering effect.

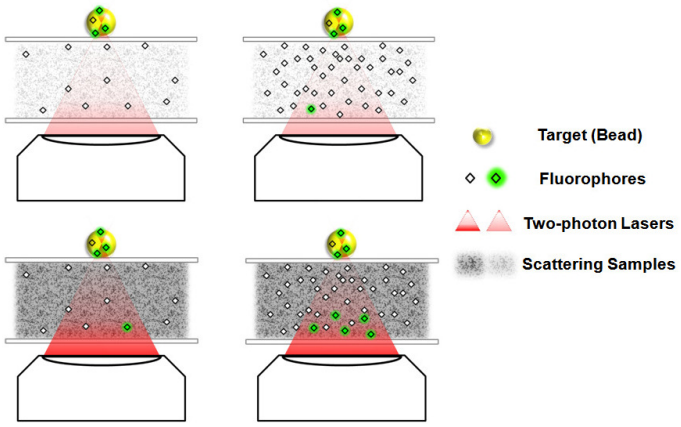

Fig. 6. The "two-layer" sample design for beads imaging experiments. Fluorescent beads were placed on a glass coverslip as the target, while a thick layer of mixed fluorescein dye solution with scattering intralipid was inserted as the background between the target and the objective. From left to right, the background fluorescein concentration increases; from top to bottom, the scattering intralipid percentage increases. The signal-to-background ratio decreases with the increase of both the background scattering and the background dye concentration.

#166548 - $15.00 USD Received 12 Apr 2012; revised 18 Jun 2012; accepted 19 Jun 2012; published 30 Jul 2012
(C) 2012 OSA

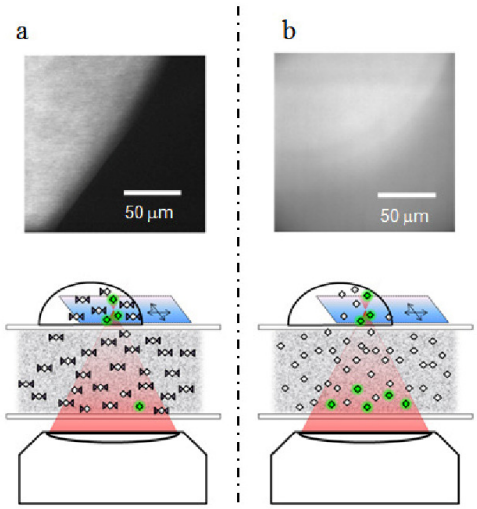

Fig. 7. The "two-layer" sample design for droplet imaging experiments. (a): imaging with caged fluorescein (Fig. 4f). (b): imaging with regular fluorescein (Fig. 4e). Images were taken across the boundaries of caged-fluorescein or regular fluorescein droplets on top of a layer of caged-fluorescein or regular fluorescein solution doped with scattering polystyrene beads.

3.2 Fluorescence imaging

All the two-photon fluorescence images were taken on a Leica TCS SP5 MP inverted microscope equipped with a Mai Tai HP laser (690-1040 nm tunable emission) and a HCX PL APO CS 20X DRY microscope objective (N.A. 0.70). A non-descanned epi PMT detector placed directly behind the objective was used for fluorescence collection in combination with a 680/SP emission filter. Images were processed with LAS AF software unless otherwise stated. Images of fluorescent beads (Figs. 1 and 2) were taken under 750 nm with a pixel dwell time of ~2.4 μs. Images of caged-fluorescein-based samples (Fig. 4d and 4f) were taken under 750 nm (48mW) with a pixel dwell time of 977 μs to achieve effective uncaging. Images of *E. coli* expressing regular GFP (Fig. 5b) were taken under 920 nm (65mW) with a pixel dwell time of 98 μs. Images of *E. coli* expressing pa-GFP (Fig. 5c) were taken under 920 nm (65mW) after 3 frames of two-photon activation under 830 nm (95 mW) with a pixel dwell time of 98 μs. Note that for tissue phantoms labeled with caged fluorescein or pa-GFP, due to the sample scattering, the actual laser power reached at the deep focal plane is much lower than the measured total power. All images were acquired with 512 by 512 pixels.

4. Conclusion

To summarize, we have presented the application of PAFs in extending the fundamental imaging-depth limit of multiphoton fluorescence microscopy. This represents a novel strategy compared to the existing approaches that focus on reducing sample scattering. Theoretical framework has been provided to describe both the dynamic and static PAFs during image acquisition. Experimentally, we demonstrated MPAI on scattering tissue phantoms labeled with caged fluorescein (dynamic PAFs scenario) or pa-GFP (static PAFs scenario), which serves as an example of synthetic small-molecule and genetically encoded PAF, respectively.

The practical performance of MPAI can be potentially improved by using PAFs with better designed photophysical properties. First, two-photon photo-activation could be much faster for molecules with larger activation cross sections. For instance, caged coumarin has been shown to exhibit 100 times faster uncaging rate via substrate-assisted photolysis [28]. Second, after being photo-activated, many photochromic fluorophores can also be switched off either thermally or by light [23, 29,30]. Such a switching-off property could re-set PAFs

#166548 - $15.00 USD Received 12 Apr 2012; revised 18 Jun 2012; accepted 19 Jun 2012; published 30 Jul 2012
(C) 2012 OSA

in the entire sample and hence allow repeated imaging on the same x-y plane or navigating through multiple layers.

It does not seem to be a mere coincidence that PAFs can play key roles for both breaking the diffraction-limited spatial resolution of fluorescence microscopy and extending the fundamental imaging-depth limit of multiphoton microscopy. In parallel, it is noteworthy to compare this work to stimulated emission reduced fluorescence (SERF) microscopy which was recently proposed for extending the fundamental imaging-depth limit of two-photon imaging [31]. While SERF microscopy is reminiscent of STED microscopy, the PAFs approach presented here can be considered as being related to PALM in terms of harnessing photo-activation. In essence, the coarse spatial resolution and the superficial penetration depth are both rooted in the difficulty of distinguishing identical molecules in space. By offering the additional disparity of (on-off) molecular quantum states, PAFs render the capability of circumventing both resolution and penetration limits.

Acknowledgments

Zhixing Chen, Lu Wei and Xinxin Zhu contributed equally to this work. We thank Ya-Ting Kao, Fang Xu, Louis Brus, Rafael Yuste, Nicholas Turro, Virginia Cornish, Darcy Peterka, Christophe Dupre and Miguel Jimenez for helpful discussions. We are grateful to Virginia Cornish for sharing lab equipments and Keith Yeager for assistance on Leica microscope. W.M. acknowledges the startup funds from Columbia University, and grant support from Kavli Institute for Brain Science.

#166548 - $15.00 USD Received 12 Apr 2012; revised 18 Jun 2012; accepted 19 Jun 2012; published 30 Jul 2012
(C) 2012 OSA

131.215.225.136 {ts '2018-11-19 13:29:22'}